## COMMUNICATION

# Surfactant-stripped naphthalocyanines for multimodal tumor theranostics with upconversion guidance cream†

Yumiao Zhang,[a,b] Hao Hong,[c] Boyang Sun,[a,b] Kevin Carter,[a] Yiru Qin,[a] Wei Wei,[d] Depeng Wang,[a] Mansik Jeon,[e] Jumin Geng,[a] Robert J. Nickles,[f] Guanying Chen,[d,g] Paras N. Prasad,[d] Chulhong Kim,[h] Jun Xia,[a] Weibo Cai[f] and Jonathan F. Lovell*[a,b]

Surfactant-stripped, nanoformulated naphthalocyanines (nano-naps) can be formed with Pluronic F127 and low temperature membrane processing, resulting in dispersed frozen micelles with extreme contrast in the near infrared region. Here, we demonstrate that nanonaps can be used for multifunctional cancer theranostics. This includes lymphatic mapping and whole tumor photoacoustic imaging following intradermal or intravenous injection in rodents. Without further modification, pre-formed nanonaps were used for positron emission tomography and passively accumulated in subcutaneous murine tumors. Because the nanonaps used absorb light beyond the visible range, a topical upconversion skin cream was developed for anti-tumor photothermal therapy with laser placement that can be guided by the naked eye.

## Introduction

Recent advances in nanoscale technologies have enabled the engineering of functional materials with a capacity for multiple integrated biomedical imaging and therapeutic modalities in one nanoparticle.[1–4] One area of interest for these materials is in photothermal therapy (PTT), an emerging ablative technique that can make use of light-absorbing exogenous contrast agents to enhance target tissue heating upon laser irradiation. Numerous PTT contrast agents have been proposed including gold nanomaterials,[5–9] carbon based nanomaterials (*e.g.* graphenes and carbon nanotubes)[10–13] and others such as CuS[14,15] and Pd[16,17] nanomaterials and others.[18,19] Organic or polymeric nanoparticles have also been explored.[20,21] For the design of photoacoustic and photothermal agents, strong absorption in near infrared (NIR) is desired, since this wavelength minimizes light scattering and absorption by endogenous biological tissues. Multimodal imaging has also gained recent attention, since nanoparticulate agents have enabling properties in this regard.[22–26] Fused imaging combinations can combine computed tomography (CT), positron emission tomography (PET), fluorescence (FL) analysis, magnetic resonance imaging (MRI), and single photon emission CT (SPECT), and representative examples include CT/PET,[27] CT/PET/SPECT,[28] MRI/CT/upconversion,[29] FL/MR/PET,[30] MRI/FL,[31] PET/FL,[32] PET/MRI,[33] and other upconversion based fused imaging modalities.[34–39] Image-guided therapy has also developed since information gathered from imaging holds potential to predict, monitor and improve therapeutic treatments.[40–44] Porphyrin and phthalocyanine molecules hold potential for applications in multimodal imaging and therapy.[45–48]

Recently our group developed a family of nanoparticles formed with a low-temperature surfactant stripping strategy, generating concentrated frozen micelles that load hydrophobic cargo with a high cargo-to-surfactant ratio.[49–51] These surfactant-stripped materials were previously demonstrated for high contrast, multimodal functional intestinal imaging. Here, we show that nanonaps also exhibit excellent behavior for cancer theranostics. Since the NIR absorbance of the nanonaps used is around 860 nm, laser placement for PTT needs to be carried out using phosphor cards or CCD displays with minimal NIR filters. While feasible, these options are not ideal for an operating room environment. To address this, a topical NaYF₄:

*[a]Department of Biomedical Engineering, University at Buffalo, State University of New York, Buffalo, New York 14260, USA. E-mail: jflovell@buffalo.edu*
*[b]Department of Chemical and Biological Engineering, University at Buffalo, State University of New York, Buffalo, New York 14260, USA*
*[c]Center for Molecular Imaging, University of Michigan, Ann Arbor, Michigan 48109, USA*
*[d]Institute for Lasers, Photonics, and Biophotonics and Department of Chemistry, University at Buffalo, State University of New York, Buffalo, New York 14260, USA*
*[e]School of Electronics Engineering, College of IT Engineering, Kyungpook National University, 702701, Korea*
*[f]Department of Radiology and Medical Physics, University of Wisconsin-Madison, Madison, Wisconsin 53705, USA*
*[g]School of Chemistry and Chemical Engineering, Harbin Institute of Technology, Harbin, Heilongjiang 150001, People's Republic of China*
*[h]Creative IT Engineering, Pohang University of Science and Technology, 790784, Korea*
†Electronic supplementary information (ESI) available. See DOI: 10.1039/c6nr09321c

Yb20%,Er2%@NaYF$_4$:Nd30% upconversion nanoparticle (UCNP) cream was successfully developed for imaging guidance during PTT.

## Experimental

Materials were obtained from Sigma unless otherwise noted. Nanonaps were formed by dissolving 1 mg 5,9,14,18,23,27,32,36-octabutoxy-2,3-naphthalocyanine (ONc) in 5 mL dichloromethane (DCM), which was then added drop-wise in 25 mL 10% (w/v) Pluronic F127 (F127), followed by stir-ring and DCM evaporation overnight. For tunable wavelength analysis, 1 mg ONc was dissolved in varying amounts of DCM (1 mL, 2 mL, 5 mL, 10 mL) and then was added dropwise to an aqueous solution of 25 mL F127 (10%, w/v). The suspension was stirred overnight and then followed by absorbance measurement. To remove free and loose Pluronic, the pre-wash nanonap solution was cooled to 4 °C and then subjected to membrane-based diafiltration (Sartorius Vivaflow, 1501008VS) assembled with a peristaltic pump (Masterflex L/S) and tubing (Materflex 6434-16) immersed in ice to reach low temperature. Absorbance was measured with a PerkinElmer Lambda 35 spectrophotometer using cuvettes with a 1 cm path length. Transmission electron microscopy was performed using a JEM-2010 electron microscope with 1% uranyl acetate staining. Dynamic light scattering was carried out with dilute nanonaps in phosphate buffered saline (PBS) using a NanoBrook 90 plus PALS instrument (Brookhaven Instruments). *In vitro* heating tests were done at a fluence rate of 1500 mW cm$^{-2}$ using an 860 nm diode laser. 1 mL of each sample was placed in a cuvette with a stir-bar, suspended over a heat sink connected to a fan, and the temperature was measured for 10 minutes of laser irradiation with a thermocouple (Atkins K-type thermo-couple, model # 39658-k). The absorbance of the samples was measured subsequently. For comparison with gold nanorods, absorption matched (at 860 nm), PEGylated gold nanorods (Nanohybrids #90228-H250UL) were compared with the same heating method.

Animal experiments were performed in accordance with the University at Buffalo or the University of Wisconsin-Madison Institutional Animal Care and Use committee. 6–8 weeks female ICR or BALB/C mice (Envigo) were used for all experiments.

For photoacoustic tomography (PAT), 75 O.D. (optical densities, that is a solution that when diluted to 1 mL would produce a calculated absorption of 75 at 860 nm) of nanonaps, equivalent to 2.6 mg of nanonaps (containing 0.6 mg ONc dye itself), were injected intravenously into mice and imaging was carried out 24 hours later, with the 860 nm excitation provided by an OPO laser (Continuum, 10 Hz pulse repetition rate, 10 ns pulse duration) which was delivered through a 1.2 cm dia-meter fiber bundle. The maximum light intensity at the skin surface was around 12 mJ cm$^{-2}$, which is below the American National Standards Institute (ANSI) safety limitation at 860 nm (42 mJ cm$^{-2}$). The photoacoustic signal was detected with a 128-element linear transducer array (5 MHz central frequency ATL/Philips L7-4). The received PA signals were amplified (by 54 dB) and digitized by using a 128-channel ultrasound data acquisition (DAQ) system (Vantage, Verasonics) with 20 MHz sampling rate. The raw channel data were reconstructed using the universal back-projection algorithm, and was displayed in real-time during experiments.

Photoacoustic lymphatics imaging was carried out using reported methods.[52,53] A custom-build volumetric reflection mode PAT system using a single element ultrasound trans-ducer was used. Tunable laser pulses were synthesized from an OPO laser (Surelite OPO PLUS; Continuum wavelength tuning range, 680 nm to 2500 nm; pulse width, 5 ns; and pulse repetition rage, 10 Hz) excited with a pump laser (SLII-10; Continuum; Q-switched Nd:YAG; 532 nm). An optical wave-length of 860 nm was used for PA imaging experiments. Generated light passed through a home-made spherical conical lens and optical condenser with a pulse energy of ~5 mJ cm$^{-2}$, much less than the safety limit. During the raster scanning for volumetric imaging, the acoustic coupling was improved with a custom-made water tray. The mice (6–8 weeks female BALB/c mouse) with 4T1 breast tumors were located below the water tray. In order to investigate the use of nano-naps for *in vivo* mapping of sentinel lymph nodes, the left axilla of a mouse was photoacoustically imaged. During *in vivo* photoacoustic imaging experiments, the mouse was under full anesthesia with a vaporized-isoflurane system. Before the injec-tion of nanonaps, the hair in the axillary regions was removed and control photoacoustic images were obtained. An intra-dermal injection of nanonaps was given on the left pad of the mouse after a control photoacoustic image was acquired. The induced PA signals were captured by using the focused ultra-sound transducer (V308; Olympus NDT; 5 MHz center fre-quency). The axial and transverse resolutions were 144 and 590 μm, respectively.

For PET imaging, $^{64}$Cu was produced *via* a $^{64}$Ni (p,n) $^{64}$Cu reaction using a CTI RDS 112 cyclotron at the University of Wisconsin-Madison. For radiolabeling, 37 MBq of $^{64}$CuCl$_2$ was diluted in 300 μL of 0.1 M sodium acetate buffer with pH of 5.5 and 400 O.D. (13.9 mg) nanonaps were added. The mixture was incubated at 37 °C for 30 min with constant shaking, fol-lowed by the purification by Amicon Ultra-4 centrifugal filter units (Millipore) using PBS. PET scanning was conducted using an Inveon microPET/microCT rodent model scanner (Siemens Medical Solutions USA, Inc.). Balb/c mice with 4T1 tumors were intravenously injected with 3.5 mg of $^{64}$Cu-labeled nanonaps, and 5–10 min static PET scans were per-formed at indicated time-points post-injection. After the last PET scans at 24 hours post injection, all the mice were eutha-nized and biodistribution studies were carried out to confirm that the quantitative tracer uptake values based on PET imaging accurately represented the radioactivity distribution in mice. Blood and major organs/tissues were collected and wet weighed. The radioactivity in the tissues or blood at different indicated time points was measured using a gamma-counter (Perkin Elmer) and presented as %ID g$^{-1}$.

For serum stability, 50% adult bovine serum was incubated with ~20 µg mL$^{-1}$ ONc nanonaps in three cuvettes. The cuvettes were incubated at 37 °C and the absorbance of each cuvette was measured at 860 nm at the indicated times. For $^{64}$Cu stability, PD-10 purified $^{64}$Cu ONc nanonaps were incubated in complete mouse serum at 37 °C for up to 24 h (the same time period used for serial PET imaging). Portions of the mixture were sampled at different time points and filtered through 100 kDa cutoff Amicon filters. The radioactivity of collected filtrates was measured in a WIZARD2 gamma counter (PerkinElmer). The percentages of retained (i.e., intact) $^{64}$Cu on nanonaps was calculated using the equation [[total radioactivity − radioactivity in filtrate)/total radioactivity × 100%].

For photothermal therapy, ICR mice bearing 4T1 tumors were injected with 75 O.D. of nanonaps, equivalent to 2.6 mg of nanonaps (containing 0.6 mg ONc dye itself). 24 hours later, a power tunable 860 nm laser diode at a fluence rate of 750 mW cm$^{-2}$ was used to treat the tumor for 3 minutes. At the same time, the temperature of the tumor was measured using a thermal camera. The tumor size was measured 3 times per week.

For NaYF$_4$:Yb20%,Er2% core UCNPs, 1 mmol RECl$_3$·6H$_2$O (RE = Y, Yb, Er) was added to a stirring flask containing 1-octadecene (15 mL) and oleic acid (7 mL), heated to 160 °C for 1 h and then cooled to room temperature. A methanol solution (10 mL) of NH$_4$F (0.148 g) and NaOH (0.1 g) was added and the temperature was increased to 120 °C. Once methanol evaporated, the mixture was heated to 300 °C for 1 h under argon. The reaction mixture was cooled to room temperature and nanoparticles were precipitated by ethanol addition, centrifu-

gation, and washing with water and ethanol prior to dispersion in hexane. Next, NaYF$_4$:Yb20%,Er2%@NaYF$_4$:Nd30% core/shell UCNPs were synthesized. The RE(CF$_3$COO)$_3$ shell precursor was synthesized by mixing Y$_2$O$_3$ (0.175 mmol) and Nd$_2$O$_3$ (0.075 mmol) with 50% trifluoroacetic acid, refluxing at 95 °C, and then evaporating the solution to dryness under argon. The NaYF$_4$:Yb20%,Er2% core nanoparticles in 10 mL hexane, Na(CF$_3$COO) (1 mmol), 10 mL oleic acid, and 10 mL 1-octadecene were combined. The mixture was heated to 120 °C for 30 min to remove hexane and water. The resulting solution was heated to 320 °C for 30 min before cooling to room temperature. 20 mL ethanol was added to precipitate the NaYF$_4$:Yb20%, Er2%@NaYF$_4$:Nd30% core/shell nanoparticles followed by centrifugation at 18 144 rcf for 7 min. These prepared UCNPs were dispersed in 10 mL hexane. For cream formation, a mixture of 5 g mineral oil, 0.7 g beeswax, 0.2 g Tween 40, and 0.8 g Atlas G-1726 beeswax derivative was prepared and preheated to 75 °C. 50 mg of UCNPs (solvent removed) were dissolved by vortexing in the heated solution, followed by slow addition of 3.3 mL of deionized water, preheated to 77 °C. The solution was stirred and the UCNP cream formed as it cooled to room temperature. For imaging guidance, UCNP cream was applied uniformly onto plastic capillary tubes or on the tumor skin prior to 860 nm laser diode irradiation.

## Results and discussion

Surfactant-stripped nanonaps were formed as previously described (Fig. 1A).[49] In brief, 5,9,14,18,23,27,32,36-octa-
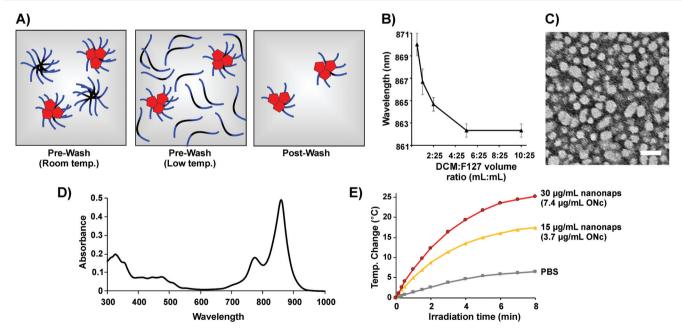


Fig. 1 Generation of surfactant-stripped octabutoxy-naphthalocyanine (ONc) nanonaps. (A) Schematic illustration of nanonap generation. ONc, F127 PPO block, and F127 PEO block are shown in red, black and blue, respectively. (B) Nanonap absorption peak as a function of the methylene chloride (DCM) to F127 solution volume ratio. (C) Negative-staining transmission electron micrograph of the ONc nanonaps (scale bar: 50 nm). (D) Absorption of 30 µg mL$^{-1}$ nanonaps in phosphate buffered saline (PBS). (E) Photothermal heating of nanonaps under 1500 mW cm$^{-2}$ 860 nm laser irradiation. The concentration of the ONc dye present within the nanonaps is indicated.

butoxy-2,3-naphthalocyanine (ONc) was dissolved in dicholoromethane (DCM) and added to a stirring 10% (w/v) Pluronic F127 solution to form micelles with evaporation of the organic solvent. The solution temperature was lowered, resulting in F127 conversion from micelles to unimers (due to the inherent behavior of Pluronics) and then a membrane process was used to strip away free and loose surfactants at low temperature, leaving concentrated, surfactant-stripped dye micelles behind with minimal F127.

As shown in Fig. 1B, the peak NIR absorption wavelength could be fine-tuned by varying the fraction of DCM (containing 1 mg ONc) added during the nanonap formation process. Presumably, the observed spectral shifts were related to a longer DCM evaporation process leading to altered stacking of ONc. As shown in Fig. 1C, nanonaps were obtained with a diameter of about 20 nm based on negative staining transmission electron microscopy. This result is in general agreement with the dynamic light scattering results, which indicated a size of 29.5 nm with a polydispersity index of 0.177 (ESI, Fig. S1†).

The absorption of ONc nanonaps, measured in phosphate buffered saline (PBS), is shown in Fig. 1D. The strong absorption peak in the near infrared was observed. Upon irradiation of a nanonap solution with an 860 nm near infrared laser diode, dose-dependent photothermal heating occurred and led to increased solution temperature (Fig. 1E). Nanonap photothermal heating effects were similar to absorption matched PEGylated gold nanorod photothermal heating (ESI, Fig. S2†). Following 10 minutes of 1500 mW cm$^{-2}$ irradiation at 860 nm, nanonaps lost approximately 25% of their NIR absorption, possibly due to the photobleaching-related phenomenon (ESI, Fig. S3†).

Next, nanonaps were examined in the context of cancer imaging applications. One area photoacoustic imaging has attracted interest is in sentinel lymph node detection for the purpose of fine needle aspiration biopsy or surgical resection.[54] Multi-color nanonaps have been demonstrated for photoacoustic lymph node imaging.[55] We confirmed that noninvasive imaging of the first draining lymph node was possible using the ONc nanonaps developed here. As shown in Fig. 2A, accumulation of nanonaps in the lymph node within 90 minutes was unambiguously observed. Thus, nanonaps have the potential to identify draining lymph nodes, which in clinical scenarios could be examined for signs of metastasis or marked for resection. Although the current generation of nanonaps is not spectrally responsive to uptake or cell binding, others have shown the potential for photoacoustic imaging with spectral shifting materials for detecting metastatic cells within the nodes.[56]

We also investigated nanonaps as an intravenously administered probe in mice bearing syngeneic subcutaneous 4T1 tumors. No signs of acute toxicity were observed at the injected doses. As shown in Fig. 2B, 24 hours after a nanonap injection of 75 O.D. (that is a solution that when diluted to a 1 mL volume would produce a calculated optical absorption of 75 at 860 nm; equivalent to 2.6 mg nanonaps, or 0.6 mg ONc dye), the photoacoustic signal delineating the tumor was clearly observed in 4T1 breast tumors, whereas in the control group not given nanonaps, no signal was seen. Photoacoustic imaging offers the possibility of resolution that examines the underlying microstructures of tumors and other biological tissues with a penetration depth of a few centimeters. On the other hand, PET is used clinically without any imaging depth
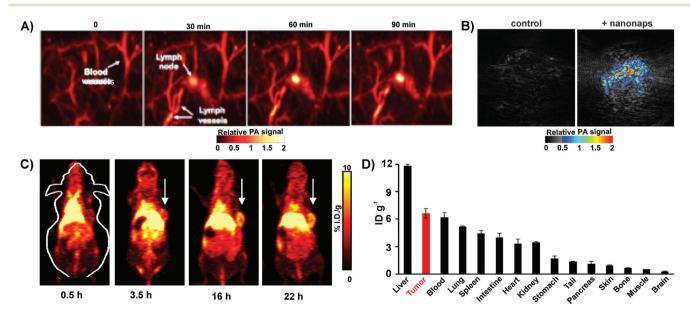


Fig. 2 Nanonaps for photoacoustic and positron emission tomography imaging. (A) Photoacoustic lymph node imaging using nanonaps. (B) Photoacoustic imaging of subcutaneous 4T1 whole tumors in living BALB/c mice with or without intravenous administration of 2.6 mg nanonaps 24 hours prior. (C) Serial PET images of 4T1 subcutaneous breast tumors in BALB/c mice after intravenous injection. Arrows show the tumor location. (D) Biodistribution of $^{64}$Cu within nanonaps 24 hours post injection of nanonaps. Mean ± std. dev. 75 optical densities at 860 nm (2.6 mg) of nanonaps were intravenously injected.

limitation, which allows for whole body imaging. The radio-isotope $^{64}$Cu readily chelated in the center of ONc, simply with incubation with the nanoparticles. An 83.2% $^{64}$Cu labeling yield (standard deviation: 10.7% for three trials) was observed with simple incubation without addition of any additional chelators. This enabled biodistribution of nanonaps and whole body imaging using positron emission tomography.

*In vitro*, ONc nanonaps were stable in serum, without any loss in absorption or loss in $^{64}$Cu chelation during incubation (ESI, Fig. S4†). Following intravenous administration to mice, the circulation half-life of nanonaps in blood was found to be ~4.5 hours by measuring the radioactivity of chelated $^{64}$Cu (ESI, Fig. S5†), which is likely influenced by the polyethylene glycol of the F127 in the exterior structure of nanonaps. As shown in Fig. 2C, after intravenous injection of labeled nanonaps, whole body PET images showed that nanonaps were taken up in 4T1 subcutaneous tumors, *via* the enhanced permeability and retention (EPR) effect. After 22 hours, tumor uptake reached 7.5 %ID g$^{-1}$ as shown by quantitative image analysis (ESI, Fig. S6A†), even though the nanonap uptake by the liver was higher than any other tissues including tumors with a radioactivity of ~16 %ID g$^{-1}$ within 22 hours (Fig. 2C and ESI, Fig. S6B†). Biodistribution of nanonaps by gamma counting of harvested organs at 24 post injection is shown in Fig. 2D. Overall, these data show that nanonaps can be used for lymphatics and tumor multimodal imaging and they exhibit reasonably high passive uptake in tumors following intravenous administration. It might be possible and advantageous to functionalize nanonaps with active targeting ligands to attempt to further enhance uptake into tumors or tumor cells. Since nanonaps are formed from Pluronic F127, other approaches reported in the literature to functionalize Pluronic with tumor targeting ligands could be applicable, which include modification with folic acid,[57–59] aptamers,[60] peptides,[61] and antibodies.[62] Functionalized Pluronic could be incorporated directly during the initial nanonap formation process, although since that involves dichloromethane emulsion and evaporation, any targeting ligands that are not stable under such conditions would need to be conjugated following nanoparticle formation and surfactant-stripping.

Based on the tumor uptake of nanonaps as shown by PET and the optical contrast deposited as shown by PAT, we next attempted PTT. Absorbers with a longer wavelength are beneficial for a deeper penetration depth, but 860 nm is beyond the visible range of eye detection so that control of the irradiation area on tumors might be an issue during laser operation. Some cameras with attenuated NIR filters are capable of detecting this emission, however in a surgical setting it might be challenging to accurately guide laser beam placement. To overcome this, we rationally designed NaYF$_4$: Yb20%,Er2%@NaYF$_4$:Nd30% core/shell structure upconversion nanoparticles (UCNPs) and then developed a topical skin cream for imaging guidance. In principle, the Nd$^{3+}$ ions in the shell have the ability to absorb light at 860 nm wavelength, and the subsequent energy transfer Nd$^{3+}$ → Yb$^{3+}$ → Er$^{3+}$ takes place (ESI, Fig. S7†), leading to the visible upconversion emission from Er$^{3+}$ in the core. As shown in Fig. 3A, photoluminescence spectra of nanocrystals dispersed in hexane at an excitation wavelength of 860 nm have emissions located at 523, 545 and 660 nm, corresponding to the $^2H_{11/2}$ → $^4I_{15/2}$, $^4S_{3/2}$ → $^4I_{15/2}$, $^4F_{9/2}$ → $^4I_{15/2}$ transitions of Er$^{3+}$, respectively. Transmission electron microscopy revealed that the average size of upconversion nanoparticles is about 25 nm (Fig. 3B). Next, we doped upconversion nanoparticles into a conventional cosmetic skin cream formulation we manufactured containing mineral oil, Tween 40 and beeswax. The texture and appearance was in line with typical cosmetic skin creams (Fig. 3C). Under laser irradiation at 860 nm, the UCNP cream (that was placed in tubes) clearly emitted visible green color that could be seen by eye (Fig. 3D).

Photothermal therapy (PTT) is based on heat generation from light-absorbers that convert light into heat upon laser irradiation at the target site. To evaluate the photothermal effect of nanonaps for cancer treatment, we injected nanonaps intravenously and 24 hours later, an 860 nm laser outputting 750 mW cm$^{-2}$ was used to irradiate 4T1 tumors for 3 minutes.
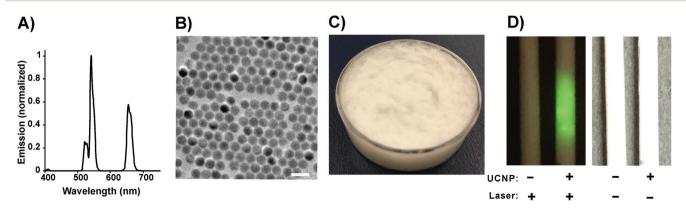


**Fig. 3** Characterization of upconversion nanoparticle (UCNP) cream for naked eye upconversion guidance of 860 nm laser placement. (A) Upconversion photoluminescence spectrum of UCNPs with laser excitation at 860 nm. (B) Transmission electron microscopy images of UCNPs (scale bar: 50 nm). (C) Bulk appearance of UCNP-doped skin cream. (D) Photographs of tubes containing cream with or without UCNP-doping under irradiation of an 860 nm laser or natural light.
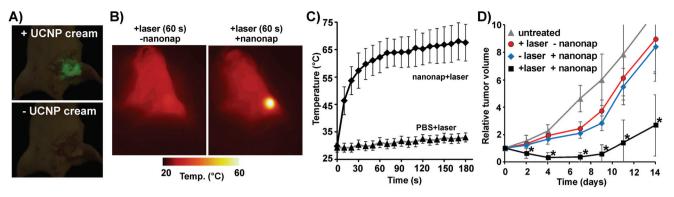
**Fig. 4** UCNP-cream-guided nanonap photothermal therapy. (A) Photographs of tumors with (top) and without (botton) upconversion cream applied on the surface of tumors with 860 nm laser irradiation. (B) Representative thermal images of mice after laser irradiation. +nanonap mice were given 2.6 mg of nanonaps intravenously (75 O.D. at 860 nm), 24 hours prior to laser treatment. (C) Tumor surface temperature during PTT laser irradiation (750 mW cm$^{-2}$ at 860 nm, 3 minutes of irradiation). All mice received UCNP cream (mean $\pm$ std. dev. for $n = 4$). (D) 4T1 tumor growth following indicated treatment ($n = 5$–6 mice per group). The asterisks show significantly reduced tumor volumes of the PTT group compared to all other groups by pair-wise two-tailed student $t$-tests ($P < 0.01$).

Upconversion cream was applied to the surface of tumors for visible guidance of the laser position. As shown in Fig. 4A, upon irradiation with an 860 nm laser, the UCNP cream emitted a bright green color that could be used to guide laser placement. According to the thermal images shown in Fig. 4B, the temperature of tumors in the nanonap group rapidly increased to over 60 °C after irradiation after 1 minute, whereas the temperature of tumors in the control group (that received laser treatment, but not nanonaps injection) almost remained unchanged. After irradiation for 3 minutes, the surface temperature reached over 65 °C, whereas a minimal temperature increase was observed for the control group (Fig. 4C). Tumors in the laser alone or nanonap alone treated groups grew to 10 times the original tumor volume after 2 weeks, whereas tumors for the laser-treated mice that received nanonaps only doubled in volume during the same time (Fig. 4D). Although these PTT treatment parameters did not permanently cure the tumors, it is conceivable that longer laser irradiation (beyond 3 minutes) would lead to improvements. As shown in Fig. S8 (ESI†), mice in the nanonap alone treated group and the laser alone treated group were sacrificed within 14 days and 18 days, respectively, whereas the nanonap and laser treated groups survived 25 days. Nanonaps exhibited statistically significant photothermal anti-tumor effects for the delay of growth of tumors based on these preliminary data with a single dose and single laser treatment.

## Conclusion

In summary, nanonaps with a tunable wavelength were used for both lymphatic and tumor photoacoustic imaging as well as PET, without any additional modifications. Nanonaps passively accumulated in subcutaneous 4T1 tumors with reasonable avidity. In order to facilitate placement of the 860 nm laser used in photothermal therapy, NaYF$_4$:Yb20%, Er2%@NaYF$_4$:Nd30% core/shell structure upconversion nano-

particles were designed and formed into a cream that enabled observation of the laser by the naked eye. Nanonaps induced significant tumor growth delay with a short 3 minute PTT treatment at 860 nm. Thus, nanonaps hold potential for anti-cancer theranostics and UCNP skin cream can provide additional guidance for laser ablation with lasers that otherwise are invisible to the naked eye.

## Author contributions

YZ and JFL conceived the idea and wrote the manuscript; YZ, BS and KC formed and characterized the nanonaps; YQ, WW, GC and PNP developed and characterized the UCNP cream, DW, MJ, CK, and JX performed photoacoustic imaging and interpreted the results; HH, RJN and WC performed PET imaging and interpreted the results; BS, KC and JG performed anti-tumor studies and interpreted the results.

## Acknowledgements

## References

1 H. Huang and J. F. Lovell, *Adv. Funct. Mater.*, 2017, **27**, 1603524.
2 J. Cheon and J.-H. Lee, *Acc. Chem. Res.*, 2008, **41**, 1630–1640.

3 F. Mao, L. Wen, C. Sun, S. Zhang, G. Wang, J. Zeng, Y. Wang, J. Ma, M. Gao and Z. Li, *ACS Nano*, 2016, **10**, 11145–11155.

4 M. Yang, Q. Fan, R. Zhang, K. Cheng, J. Yan, D. Pan, X. Ma, A. Lu and Z. Cheng, *Biomaterials*, 2015, **69**, 30–37.

5 M. S. Yavuz, Y. Cheng, J. Chen, C. M. Cobley, Q. Zhang, M. Rycenga, J. Xie, C. Kim, K. H. Song, A. G. Schwartz, L. V. Wang and Y. Xia, *Nat. Mater.*, 2009, **8**, 935–939.

6 X. Huang, S. Neretina and M. A. El-Sayed, *Adv. Mater.*, 2009, **21**, 4880–4910.

7 J. Chen, D. Wang, J. Xi, L. Au, A. Siekkinen, A. Warsen, Z.-Y. Li, H. Zhang, Y. Xia and X. Li, *Nano Lett.*, 2007, **7**, 1318–1322.

8 H. Liu, D. Chen, L. Li, T. Liu, L. Tan, X. Wu and F. Tang, *Angew. Chem., Int. Ed.*, 2011, **123**, 921–925.

9 G. von Maltzahn, J.-H. Park, A. Agrawal, N. K. Bandaru, S. K. Das, M. J. Sailor and S. N. Bhatia, *Cancer Res.*, 2009, **69**, 3892–3900.

10 Z. M. Markovic, L. M. Harhaji-Trajkovic, B. M. Todorovic-Markovic, D. P. Kepić, K. M. Arsikin, S. P. Jovanović, A. C. Pantovic, M. D. Dramićanin and V. S. Trajkovic, *Biomaterials*, 2011, **32**, 1121–1129.

11 H. K. Moon, S. H. Lee and H. C. Choi, *ACS Nano*, 2009, **3**, 3707–3713.

12 K. Yang, S. Zhang, G. Zhang, X. Sun, S.-T. Lee and Z. Liu, *Nano Lett.*, 2010, **10**, 3318–3323.

13 J. T. Robinson, K. Welsher, S. M. Tabakman, S. P. Sherlock, H. Wang, R. Luong and H. Dai, *Nano Res.*, 2010, **3**, 779–793.

14 M. Zhou, R. Zhang, M. Huang, W. Lu, S. Song, M. P. Melancon, M. Tian, D. Liang and C. Li, *J. Am. Chem. Soc.*, 2010, **132**, 15351–15358.

15 Q. Tian, M. Tang, Y. Sun, R. Zou, Z. Chen, M. Zhu, S. Yang, J. Wang, J. Wang and J. Hu, *Adv. Mater.*, 2011, **23**, 3542–3547.

16 W. Fang, S. Tang, P. Liu, X. Fang, J. Gong and N. Zheng, *Small*, 2012, **8**, 3816–3822.

17 M. Chen, S. Tang, Z. Guo, X. Wang, S. Mo, X. Huang, G. Liu and N. Zheng, *Adv. Mater.*, 2014, **26**, 8210–8216.

18 C. Kim, C. Favazza and L. V. Wang, *Chem. Rev.*, 2010, **110**, 2756–2782.

19 Y. Liu, L. Nie and X. Chen, *Trends Biotechnol.*, 2016, **34**, 420–433.

20 J. F. Lovell, C. S. Jin, E. Huynh, H. Jin, C. Kim, J. L. Rubinstein, W. C. W. Chan, W. Cao, L. V. Wang and G. Zheng, *Nat. Mater.*, 2011, **10**, 324–332.

21 Y. Lyu, C. Xie, S. A. Chechetka, E. Miyako and K. Pu, *J. Am. Chem. Soc.*, 2016, **138**, 9049–9052.

22 I.-C. Sun, D.-K. Eun, H. Koo, C.-Y. Ko, H.-S. Kim, D. K. Yi, K. Choi, I. C. Kwon, K. Kim and C.-H. Ahn, *Angew. Chem., Int. Ed.*, 2011, **50**, 9348–9351.

23 Y. Li, T. Lin, Y. Luo, Q. Liu, W. Xiao, W. Guo, D. Lac, H. Zhang, C. Feng, S. Wachsmann-Hogiu, J. H. Walton, S. R. Cherry, D. J. Rowland, D. Kukis, C. Pan and K. S. Lam, *Nat. Commun.*, 2014, **5**, 4712.

24 K. Pu, A. J. Shuhendler, J. V. Jokerst, J. Mei, S. S. Gambhir, Z. Bao and J. Rao, *Nat. Nanotechnol.*, 2014, **9**, 233–239.

25 N. Mitchell, T. L. Kalber, M. S. Cooper, K. Sunassee, S. L. Chalker, K. P. Shaw, K. L. Ordidge, A. Badar, S. M. Janes, P. J. Blower, M. F. Lythgoe, H. C. Hailes and A. B. Tabor, *Biomaterials*, 2013, **34**, 1179–1192.

26 J. Rieffel, F. Chen, J. Kim, G. Chen, W. Shao, S. Shao, U. Chitgupi, R. Hernandez, S. A. Graves, R. J. Nickles, *et al.*, *Adv. Mater.*, 2015, **27**, 1785–1790.

27 A. Iagaru, E. Mittra, D. W. Dick and S. S. Gambhir, *Mol. Imaging Biol.*, 2011, **14**, 252–259.

28 W. Koba, L. A. Jelicks and E. J. Fine, *Am. J. Pathol.*, 2013, **182**, 319–324.

29 X. Zhu, J. Zhou, M. Chen, M. Shi, W. Feng and F. Li, *Biomaterials*, 2012, **33**, 4618–4627.

30 M. Yang, K. Cheng, S. Qi, H. Liu, Y. Jiang, H. Jiang, J. Li, K. Chen, H. Zhang and Z. Cheng, *Biomaterials*, 2013, **34**, 2796–2806.

31 J. Kim, H. S. Kim, N. Lee, T. Kim, H. Kim, T. Yu, I. C. Song, W. K. Moon and T. Hyeon, *Angew. Chem., Int. Ed.*, 2008, **47**, 8438–8441.

32 W. Cai, K. Chen, Z.-B. Li, S. S. Gambhir and X. Chen, *J. Nucl. Med.*, 2007, **48**, 1862–1870.

33 H.-Y. Lee, Z. Li, K. Chen, A. R. Hsu, C. Xu, J. Xie, S. Sun and X. Chen, *J. Nucl. Med.*, 2008, **49**, 1371–1379.

34 Z. Liu, K. Dong, J. Liu, X. Han, J. Ren and X. Qu, *Small*, 2014, **10**, 2429–2438.

35 J.-W. Shen, C.-X. Yang, L.-X. Dong, H.-R. Sun, K. Gao and X.-P. Yan, *Anal. Chem.*, 2013, **85**, 12166–12172.

36 D. Yang, Y. Dai, J. Liu, Y. Zhou, Y. Chen, C. Li, P. 'an Ma and J. Lin, *Biomaterials*, 2014, **35**, 2011–2023.

37 D. Ni, W. Bu, S. Zhang, X. Zheng, M. Li, H. Xing, Q. Xiao, Y. Liu, Y. Hua, L. Zhou, W. Peng, K. Zhao and J. Shi, *Adv. Funct. Mater.*, 2014, **24**, 6613–6620.

38 Q. Xiao, W. Bu, Q. Ren, S. Zhang, H. Xing, F. Chen, M. Li, X. Zheng, Y. Hua, L. Zhou, W. Peng, H. Qu, Z. Wang, K. Zhao and J. Shi, *Biomaterials*, 2012, **33**, 7530–7539.

39 H. Xing, W. Bu, S. Zhang, X. Zheng, M. Li, F. Chen, Q. He, L. Zhou, W. Peng, Y. Hua and J. Shi, *Biomaterials*, 2012, **33**, 1079–1089.

40 J. Qiu, Q. Xiao, X. Zheng, L. Zhang, H. Xing, D. Ni, Y. Liu, S. Zhang, Q. Ren, Y. Hua, K. Zhao and W. Bu, *Nano Res.*, 2015, **8**, 3580–3590.

41 L. Cheng, J. Liu, X. Gu, H. Gong, X. Shi, T. Liu, C. Wang, X. Wang, G. Liu, H. Xing, W. Bu, B. Sun and Z. Liu, *Adv. Mater.*, 2014, **26**, 1886–1893.

42 K. Yang, L. Hu, X. Ma, S. Ye, L. Cheng, X. Shi, C. Li, Y. Li and Z. Liu, *Adv. Mater.*, 2012, **24**, 1868–1872.

43 X. Song, H. Gong, S. Yin, L. Cheng, C. Wang, Z. Li, Y. Li, X. Wang, G. Liu and Z. Liu, *Adv. Funct. Mater.*, 2014, **24**, 1194–1201.

44 J. Xia, C. Kim and J. F. Lovell, *Curr. Drug Targets*, 2015, **16**, 571–581.

45 H. Huang, W. Song, J. Rieffel and J. F. Lovell, *Front. Phys.*, 2015, **3**, 23.

46 Y. Zhang and J. F. Lovell, *Theranostics*, 2012, **2**, 905–915.

47 Y. Zhou, D. Wang, Y. Zhang, U. Chitgupi, J. Geng, Y. Wang, Y. Zhang, T. R. Cook, J. Xia and J. F. Lovell, *Theranostics*, 2016, **6**, 688–697.

48 Y. Zhang and J. F. Lovell, *Wiley Interdiscip. Rev.: Nanomed. Nanobiotechnol.*, 2017, **9**, e1420.

49 Y. Zhang, M. Jeon, L. J. Rich, H. Hong, J. Geng, Y. Zhang, S. Shi, T. E. Barnhart, P. Alexandridis, J. D. Huizinga, M. Seshadri, W. Cai, C. Kim and J. F. Lovell, *Nat. Nanotechnol.*, 2014, **9**, 631–638.

50 Y. Zhang, D. Wang, S. Goel, B. Sun, U. Chitgupi, J. Geng, H. Sun, T. E. Barnhart, W. Cai, J. Xia and J. F. Lovell, *Adv. Mater.*, 2016, **28**, 8524–8530.

51 Y. Zhang, W. Song, J. Geng, U. Chitgupi, H. Unsal, J. Federizon, J. Rzayev, D. K. Sukumaran, P. Alexandridis and J. F. Lovell, *Nat. Commun.*, 2016, **7**, 11649.

52 M. Jeon, J. Kim and C. Kim, *Med. Biol. Eng. Comput.*, 2016, **54**, 283–294.

53 C. Kim, M. Jeon and L. V. Wang, *Opt. Lett.*, 2011, **36**, 3599–3601.

54 A. Garcia-Uribe, T. N. Erpelding, A. Krumholz, H. Ke, K. Maslov, C. Appleton, J. A. Margenthaler and L. V. Wang, *Sci. Rep.*, 2015, **5**, 15748.

55 C. Lee, J. Kim, Y. Zhang, M. Jeon, C. Liu, L. Song, J. F. Lovell and C. Kim, *Biomaterials*, 2015, **73**, 142–148.

56 S. Mallidi, T. Larson, J. Tam, P. P. Joshi, A. Karpiouk, K. Sokolov and S. Emelianov, *Nano Lett.*, 2009, **9**, 2825–2831.

57 F. Liu, J.-Y. Park, Y. Zhang, C. Conwell, Y. Liu, S. R. Bathula and L. Huang, *J. Pharm. Sci.*, 2010, **99**, 3542–3551.

58 L. Liu, K.-T. Yong, I. Roy, W.-C. Law, L. Ye, J. Liu, J. Liu, R. Kumar, X. Zhang and P. N. Prasad, *Theranostics*, 2012, **2**, 705–713.

59 J.-J. Lin, J.-S. Chen, S.-J. Huang, J.-H. Ko, Y.-M. Wang, T.-L. Chen and L.-F. Wang, *Biomaterials*, 2009, **30**, 5114–5124.

60 X. Li, Y. Yu, Q. Ji and L. Qiu, *Nanomedicine*, 2015, **11**, 175–184.

61 J.-Y. Kim, W. I. Choi, Y. H. Kim and G. Tae, *Biomaterials*, 2013, **34**, 1170–1178.

62 H. Ding, K.-T. Yong, W.-C. Law, I. Roy, R. Hu, F. Wu, W. Zhao, K. Huang, F. Erogbogbo, E. J. Bergey and P. N. Prasad, *Nanoscale*, 2011, **3**, 1813–1822.